MIT Open Access Articles

Modeling and Estimating Current Harmonics of Variable Electronic Loads

Modeling and Estimating Current Harmonics of Variable Electronic Loads

Warit Wichakool, *Student Member, IEEE*, Al-Thaddeus Avestruz, *Student Member, IEEE*,
Robert W. Cox, *Member, IEEE*, and Steven B. Leeb, *Fellow, IEEE*

Abstract—**This paper develops a model for relating input current harmonic content to real power consumption for variable electronic loads, specifically for loads' actively controlled inverters energized by an uncontrolled rectification of the utility. This model serves as the basis for a method for estimating and disaggregating the power consumption of variable speed drives (VSDs) and rectifier loads from other constant power loads. This method can be used for nonintrusive power monitoring. The approach described in this paper uses the approximate switching function of the rectifier to derive the best estimating function for the fundamental current harmonic from a finite set of current harmonics uniquely associated with the operation of the drive. Experimental results show that the proposed VSD power and harmonic estimator can track VSD power consumption for monitoring given knowledge or an estimate of the input current harmonic content.**

Index Terms—**Rectifiers, spectral analysis, switching functions, variable speed drives.**

I. INTRODUCTION

SUBSTANTIAL and successful efforts have been made to develop models that predict the input current harmonics of continuously variable electronic loads such as variable speed drives (VSDs) and rectifier loads, given an assumed operating point in real power consumption [1]–[9]. Specifically, given an assumed or known level of real power consumption and circuit parameters, it is possible to predict the harmonic currents consumed by a variable speed drive. For many applications, it would be convenient and even enabling to have an analytical approach to the inverse problem [10], [11]. That is, a means to model and predict the real power consumption of a drive, given an observed or estimated line current harmonic pattern, would open the door to new power monitoring and also modeling techniques for constraining motor-drive design problems. This paper develops mathematical models that accurately predict real power consumption from measured or estimated input harmonic levels.

These methods can be used, for example, to determine the maximum shaft power available to a drive, given specific limits or regulatory requirements on a pattern of input current har-

monics. The models developed here can also be used to track and disaggregate the real power consumption of VSDs and rectifier loads given observations of harmonic currents. This type of modeling enables the development of "smart" or nonintrusive electric metering solutions. nonintrusive "smart" metering can determine the operating schedule of a collection of electrical loads strictly from measurements made at the electric utility service entry powering a collection of loads [12]. A nonintrusive load monitoring (NILM) system tracks the operating condition and power consumption of multiple loads using line current harmonic signatures or spectral envelopes [10]–[14]. For a constant power load, the identification is accomplished by searching the aggregate set of current harmonic signatures or spectral envelopes for the appropriate combination of characteristic transient patterns and steady-state power changes [11], [12]. Continuously, variable loads like variable speed drives (VSDs) do not have a unique current harmonic signature, and can confound the existing nonintrusive power-monitoring scheme. The harmonic inverse model presented here can allow the nonintrusive load monitoring system to track and disaggregate the variable power consumption of variable speed drives and rectifiers from telltale harmonic signatures.

In general, VSDs are used to optimize energy consumption and controllability in many industrial and commercial facilities. A typical VSD system consists of a rectifier, a dc-bus link, an inverter, and an induction motor. A rectifier front-end of the VSD usually draws current that is rich in harmonic content. These line harmonics can be used to identify and track the VSD load. A VSD power estimator has been developed using correlation functions between the fundamental and higher harmonics of the measured current [11]. Although this curve-fitting approach provides a simple way for extracting the harmonic content of the VSD from the aggregate measurements, the correlation functions used in this black-box approach can change as much as ten percents from the base case [10]. Variation in the input voltage can affect the relative amount of harmonic content consumed by the rectifier [5]. A more accurate model that incorporates system behaviors could provide insights and improvements in estimating power consumption of the VSD using current harmonics.

One analytical technique that provides a closed form solution for the current harmonics drawn by rectifiers uses a switching-function approach [1], [3], [7]–[9]. By studying the switching-function method, a nonintrusive load monitoring (NILM) system can approximate linear relationships among current harmonics consumed by the rectifier front-end without knowing exact operating conditions and all circuit parameters of the
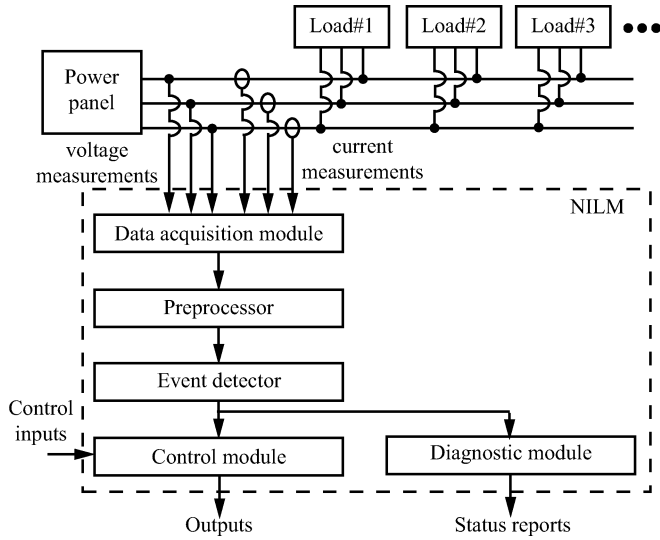
Fig. 1.   Block diagram of the nonintrusive load monitoring system.

VSD. This derived relationship allows the system to accurately predict the real power consumption of variable speed drives.

This paper proposes a switching-function-based power estimator that can uniquely resolve the power consumption of VSDs energized by an uncontrolled rectification of the utility from aggregate current measurements under varying input voltage conditions. The paper is organized as follows. First, the NILM system is briefly explained in Section II. Section III introduces a general VSD model. A brief summary of the switching-function method is covered in Section IV. The switching-function-based estimator is derived in Section V. Experimental results are shown in Section VI. Finally, the proposed estimator is summarized in Section VII.

II. BACKGROUND

An NILM system monitors multiple loads from a central observation point and extracts information about each load from current and voltage waveforms. The system block diagram is shown in Fig. 1. The system computes short-time Fourier series coefficients or spectral envelopes from the measured phase currents and voltages. These coefficients are used to track and disaggregate each load from aggregate measurements [12], [14]. Fourier series coefficients can be computed as follows. Let $v(t) = V_1 \sin(2\pi t/T)$ be a reference voltage and the variable T represents the fundamental period. Given a line current $i(t)$, the in-phase and quadrature components of the kth harmonic are denoted by $I_k^p(t)$ and $I_k^q(t)$, respectively. These coefficients can be computed by

$$I_k^p(t) = \frac{2}{T} \int_{t-T}^{t} i(\tau) \sin\left(\frac{2\pi k}{T}\tau\right) d\tau \tag{1}$$

and

$$I_k^q(t) = \frac{2}{T} \int_{t-T}^{t} i(\tau) \cos\left(\frac{2\pi k}{T}\tau\right) d\tau. \tag{2}$$
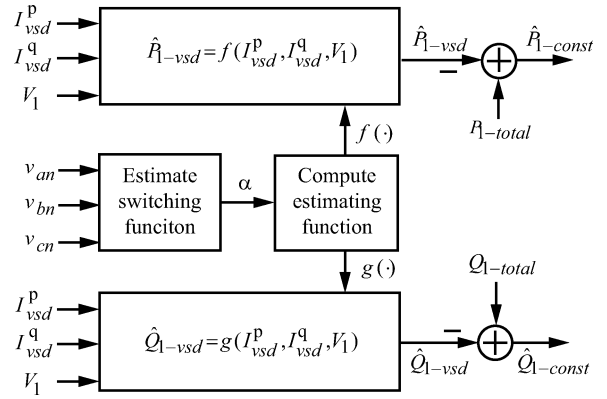

Fig. 2.   Block diagram of the switching-function-based VSD power estimator.

In steady-state operation, the fundamental real and reactive powers can be computed by

$$P_1(t) = \frac{1}{2} V_1 I_1^p(t) \tag{3}$$

and

$$Q_1(t) = \frac{1}{2} V_1 I_1^q(t) \tag{4}$$

respectively. When VSDs are included in the group of monitored loads, the time-varying nature of their power consumption can affect the power consumption patterns of other loads. Consequently, the load recognition system may not properly match signatures.

To improve the capability of the NILM system, the VSD power estimator, shown in Fig. 2, has been developed. Note that it uses the input voltage to approximate a feasible switching function and to create estimating functions for the fundamental current consumed by the VSD from a finite set of higher harmonics uniquely associated with the drive. Finally, the estimator computes the fundamental real and reactive powers consumed by the VSD using (3) and (4), respectively, for all three phases. Specifically, the estimated fundamental real and reactive powers of the three-phase load can be computed by

$$\widehat{P}_{1-\text{VSD}} = V_1^a \widehat{I}_1^{pa} + V_1^b \widehat{I}_1^{pb} + V_1^c \widehat{I}_1^{pc} \tag{5}$$

and

$$\widehat{Q}_{1-\text{VSD}} = V_1^a \widehat{I}_1^{qa} + V_1^b \widehat{I}_1^{qb} + V_1^c \widehat{I}_1^{qc} \tag{6}$$

respectively. Variables $\widehat{I}_1^{pa}$ and $\widehat{I}_1^{qa}$ represent the estimated in-phase and quadrature components of the fundamental current harmonic consumed by the VSD in phase-A. Superscripts a, b, and c indicate the phase of currents and voltages. Sections below describe the operation of the VSD and present a method for estimating and removing the harmonic currents consumed by the VSD.

III. VSD MODEL

A simple circuit topology that represents a VSD system with an uncontrolled rectifier is shown in Fig. 3 [5]. A dc-bus capacitor is used to minimize the voltage ripple. An optional dc-bus inductor can be installed to reduce the peak current. The inverter
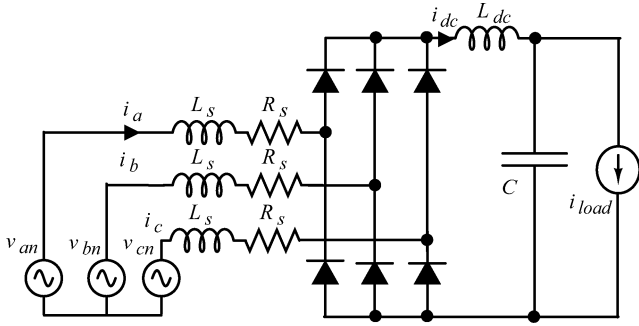
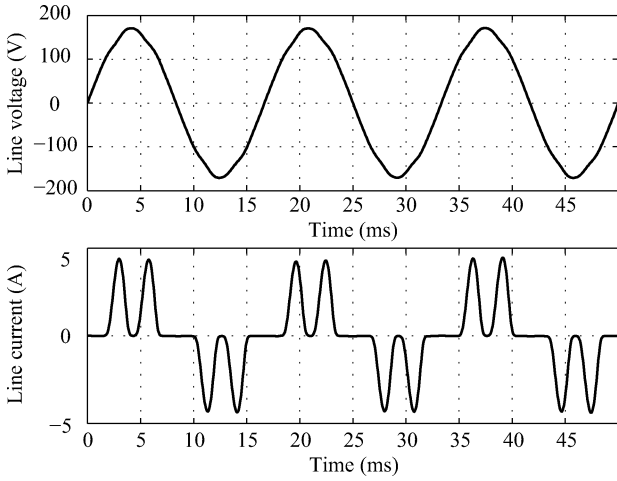Fig. 3.   Circuit model of the VSD equipped with an uncontrolled rectifier.

Fig. 4.   Typical line current and reference input voltage waveforms consumed by a VSD.
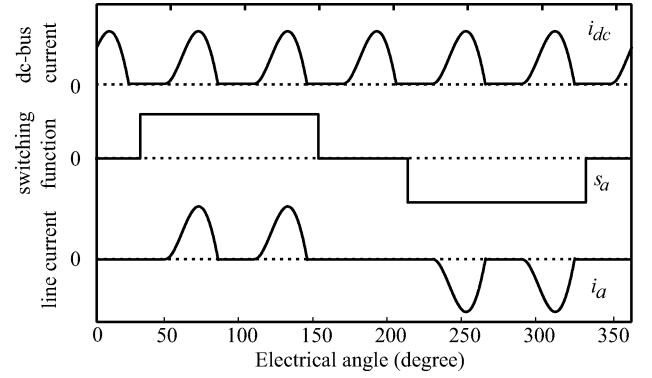

Fig. 5.   Examples of the dc-bus current, the switching function, and the ac-side current when the input voltages are balanced and the system is in a steady state.

is normally operated at a frequency well above line frequency, so any harmonics it produces are generally negligible at the ac side [6]. Simulation results show that the constant current source i_{load} provides a good model for the inverter–motor combination [5]. As a result, the model shown in Fig. 3 provides a good representation of the VSD system for simulation and initial verification purposes.

A typical ac-side line current consumed by a VSD with an uncontrolled rectifier exhibits two separate peaks during each half cycle as shown in Fig. 4. In this discontinuous conduction mode (DCM), the measured current mainly consists of the fundamental and a series of odd harmonics, i.e., 3rd, 5th, 7th, 9th, 11th, and 13th. Assuming these higher harmonics are uniquely associated with the VSD, they can be used to estimate the fundamental current harmonic and the fundamental power consumed by the VSD as shown in Fig. 2.

IV. SWITCHING-FUNCTION METHOD

This section uses the switching-function technique to briefly explain the consumption of line current harmonics by VSDs with uncontrolled rectifiers. Let the observed line-to-neutral voltage on phase-A, $v_{an}(\theta) = V_1 \sin\theta$, be a reference voltage, where $\theta \in [0, 2\pi)$ is an electrical angle and V_1 is the magnitude of the fundamental. During each voltage cycle, the observed phase-A

current, $i_a(\theta)$, is the result of the modulation of the dc-side current, $i_{\text{dc}}(\theta)$, by the corresponding switching function, $s_a(\theta)$. The switching function represents the on/off times of the switches in the rectifier. Examples of current and switching-function waveforms are shown in Fig. 5. Mathematically, phase-A line current is given by

$$i_a(\theta) = s_a(\theta) i_{\text{dc}}(\theta). \tag{7}$$

Each variable in (7) can be represented in terms of in-phase and quadrature components using Fourier analysis. The line current is the result of the convolution between the switching function and the dc-bus current [1]. The line current is represented as

$$i_a(\theta) = I_0 + \sum_k \left(I_k^p \sin k\theta - I_k^q \cos k\theta \right) \tag{8}$$

where the variable k represents a harmonic number, the variable I_0 is the dc component of the line current, and the variables I_k^p and I_k^q are the magnitudes of the in-phase and quadrature components of the line-side kth current harmonic, respectively. An arbitrary switching function can also be represented as

$$s_a(\theta) = S_0 + \sum_n \left(S_n^p \sin n\theta - S_n^q \cos n\theta \right) \tag{9}$$

where the variable n is the harmonic number, the variable S_0 is the dc component, and the variables S_n^p and S_n^q represent the magnitudes of the in-phase and quadrature components of the nth harmonic of the switching function, respectively. Similarly, the dc-bus current can be represented by another Fourier series as

$$i_{\text{dc}}(\theta) = I_0^{\text{dc}} + \sum_m \left(I_m^{p-\text{dc}} \cos m\theta + I_m^{q-\text{dc}} \sin m\theta \right) \tag{10}$$

where the variable m is the harmonic number, the variable I_0^{dc} is the dc component, and the variables $I_m^{p-\text{dc}}$ and $I_m^{q-\text{dc}}$ represent the magnitudes of the in-phase and quadrature components of the mth harmonic of the dc-side current, respectively.

Alternatively, each Fourier series coefficient of the phase current can be written in terms of a weighted sum of the dc-side Fourier series coefficients by substituting (9) and (10) in (7). Mathematically, Fourier series coefficients I_0, I_k^p, and I_k^q are

given by

$$I_0 = W_0^{0p} I^{p-\mathrm{dc}} + W_0^{0q} I^{q-\mathrm{dc}} \tag{11}$$

$$I_k^p = W_k^{pp} I^{p-\mathrm{dc}} + W_k^{pq} I^{q-\mathrm{dc}} \tag{12}$$

and

$$I_k^q = W_k^{qp} I^{p-\mathrm{dc}} + W_k^{qq} I^{q-\mathrm{dc}}. \tag{13}$$

The column vector $I^{p-\mathrm{dc}}$ represents the dc and the in-phase components of the dc-side harmonics, i.e.

$$I^{p-\mathrm{dc}} = \begin{bmatrix} I_0^{\mathrm{dc}} & I_1^{p-\mathrm{dc}} & I_2^{p-\mathrm{dc}} & I_3^{p-\mathrm{dc}} & \dots \end{bmatrix}^T$$

and a column vector I_{dcq} represent the quadrature components of the dc-side harmonics, i.e.

$$I^{q-\mathrm{dc}} = \begin{bmatrix} I_1^{q-\mathrm{dc}} & I_2^{q-\mathrm{dc}} & I_3^{q-\mathrm{dc}} & \dots \end{bmatrix}^T.$$

Row vectors W_0^{0p} and W_0^{0q} contain the weighting coefficients that relate the in-phase and quadrature components of the dc-side harmonics to the dc component of the line-side current, respectively. The row vector W_k^{pp} relates the in-phase components of the dc-side harmonics to the in-phase component of the line-side kth harmonic. The row vector W_k^{pq} relates the quadrature components of the dc-side harmonics to the in-phase component of the line-side kth harmonic. The row vector W_k^{qp} relates the in-phase components of the dc-side harmonics to the quadrature component of the line-side kth harmonic. The row vector W_k^{qq} relates the quadrature components of the dc-side harmonics to the quadrature component of the line-side kth harmonic. These weighting coefficients can be easily computed from switching-function coefficients, S_0, S_n^p, and S_n^q. The computations of these coefficients are included in Appendix. Once both the switching function and the dc-side harmonics have been estimated, all VSD line-side harmonics can be computed using (11)–(13).

V. ESTIMATOR DERIVATION

In the load identification problem, the dc-bus current and the switching function are generally not observable in the aggregate measurements. Few approximations must be applied in order to relate higher current harmonics to the fundamental harmonic consumed by the VSD. The derivation of the proposed estimator can be divided into two parts: the estimation of the switching function and the estimation of the dc-side current harmonics. In this paper, the following conditions are assumed.

1) The rectifier front-end is operated in a DCM.
2) Each diode behaves like an ideal switch.
3) Harmonics used in the estimator are uniquely consumed by the VSD.

A. Switching-Function Approximation

The actual switching function is defined by switching instants of the diode bridge and is not always observable in the aggregate measurement. In DCM, intersections between line voltages can be used to estimate the switching functions of the line currents because phase currents do not commutate during switching instants. In this paper, the approximate switching function is the
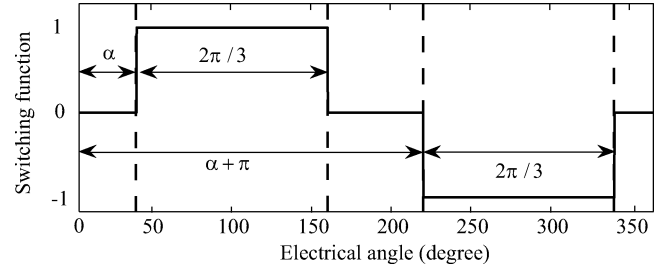

Fig. 6.   Approximate switching function.

shifted ideal switching function that can be expressed as

$$s_a(\theta) = \begin{cases} 1, & \text{for } \alpha \le \theta \le \alpha + \dfrac{2\pi}{3} & \text{(14a)} \\[2mm] -1, & \text{for } \alpha + \pi \le \theta \le \alpha + \dfrac{5\pi}{3} & \text{(14b)} \\[2mm] 0, & \text{otherwise} & \text{(14c)} \end{cases}$$

where the angle α is the minimum angle that allows the shifted ideal switching function to contain all four pulses for phase-A. An example of the approximate switching function is shown in Fig. 6. Fourier series coefficients S_n^p and S_n^q of the approximate switching function in (14) are given by

$$S_n^p = -\frac{4}{n\pi} \sin \frac{n\pi}{2} \sin \frac{n\pi}{3} \cos n \left(\frac{5\pi}{6} + \alpha \right) \tag{15}$$

and

$$S_n^q = -\frac{4}{n\pi} \sin \frac{n\pi}{2} \sin \frac{n\pi}{3} \sin n \left(\frac{5\pi}{6} + \alpha \right). \tag{16}$$

In this case, weighting coefficients vectors $W_k^{pp}, W_k^{pq}, W_k^{qp}$, and W_k^{qq} contain many zero coefficients. For example, the weighting coefficient matrix for the fundamental current harmonic W_1^{pp} is given by

$$W_1^{pp} = \begin{bmatrix} w_{1,0}^{pp}, & 0, & w_{1,2}^{pp}, & 0, & w_{1,4}^{pp}, & 0, & \dots \end{bmatrix}.$$

Furthermore, all line-side triplen harmonics only depend on dc-side even harmonics that are not multiple of six. For example, the weighting vector for the third harmonic W_3^{pp} is given by

$$W_3^{pp} = \begin{bmatrix} \mathbf{0}, & 0, & w_{3,2}^{pp}, & 0, & w_{3,4}^{pp}, & 0, & \mathbf{0}, & 0, & w_{3,8}^{pp}, & \dots \end{bmatrix}.$$

Finally, the kth ac-side harmonic is primarily caused by the $(k-1)$th and $(k+1)$th dc-side harmonics when the shifted, ideal switching function shown above is used. These properties can be used to further simplify the estimation problem.

B. Effects of DC-Side Harmonics

In the ideal case, the input voltage is balanced and the inverter reaches steady state. In this case, the dc-side current consists of six identical pulses per line cycle. As a result, the dc-side current contains only the dc component and harmonics that are multiples of six. Examples of current and switching function waveforms in the ideal case are shown in Fig. 5. In this case, harmonic vectors $I^{p-\mathrm{dc}}$ and $I^{q-\mathrm{dc}}$ can be reduced to $[I_0^{\mathrm{dc}}, I_6^{p-\mathrm{dc}}, I_{12}^{p-\mathrm{dc}}, \dots]^T$ and $[I_6^{q-\mathrm{dc}}, I_{12}^{p-\mathrm{dc}}, I_{18}^{p-\mathrm{dc}}, \dots]^T$, respectively. In general, the rectifier has a dc-bus filter to smooth out the current and suppress

higher harmonics. Theoretically, each current pulse in Fig. 5 can be assumed to be a square pulse. In this case. the magnitude of the dc-side mth harmonic would be proportional to $1/m$ according to Fourier series coefficients. Furthermore, the approximated switching function shown in Fig. 6 also attenuates higher harmonics according to Fourier series coefficients computed in (15) and (16). As a result, the effect of the dc-side higher harmonics on the ac-side low harmonics is further reduced. As a result, higher harmonics can be ignored. The effect of neglecting higher harmonics can be computed quantitatively by the comparing the $\mathcal{L}_2$ norm of the unused higher harmonics and the retained harmonics to ensure that the approximation error is reasonably small in any specific application context.

Consequently, the harmonic vectors $I^{p-\mathrm{dc}}$ and $I^{q-\mathrm{dc}}$ can be divided into two parts: main and residual harmonics. Main harmonics include the first M entries of dc-side harmonic vectors represented by

$$I^{p-\mathrm{dc}M} = [\overbrace{I_0^{\mathrm{dc}}, I_6^{p-\mathrm{dc}}, I_{12}^{p-\mathrm{dc}}, \ldots}^{\text{M terms}}]$$

and

$$I^{q-\mathrm{dc}M} = [\overbrace{I_6^{q-\mathrm{dc}}, I_{12}^{q-\mathrm{dc}}, I_{18}^{q-\mathrm{dc}}, \ldots}^{\text{M terms}}].$$

Residual harmonics include all other higher harmonics represented by

$$\Delta I^{p-\mathrm{dc}M} = [I_{6M}^{p-\mathrm{dc}}, I_{6(M+1)}^{p-\mathrm{dc}}, I_{6(M+2)}^{p-\mathrm{dc}}, \ldots]$$

and

$$\Delta I^{q-\mathrm{dc}M} = [I_{6(M+1)}^{q-\mathrm{dc}}, I_{6(M+2)}^{q-\mathrm{dc}}, I_{6(M+3)}^{q-\mathrm{dc}}, \ldots].$$

In this case, the ac-side fundamental harmonic components can be approximated as

$$\begin{bmatrix} I_1^p \\ \hline I_1^q \end{bmatrix} \approx \left[\begin{array}{c|c} W_1^{pp-M} & W_1^{pq-M} \\ \hline W_1^{qp-M} & W_1^{qq-M} \end{array} \right] \begin{bmatrix} I^{p-\mathrm{dc}M} \\ \hline I^{q-\mathrm{dc}M} \end{bmatrix} \quad (17)$$

where block matrices W_1^{pp-M}, W_1^{pq-M}, W_1^{qp-M}, and W_1^{qq-M} contain M coefficients that correspond to M harmonics used in the vector $I^{p-\mathrm{dc}M}$ and $I^{q-\mathrm{dc}M}$ for the fundamental ac-side harmonic I_1^p and I_1^q. Similarly, higher order, ac-side current harmonics consumed by the VSD can be expressed as

$$\begin{bmatrix} I_{\mathrm{VSD}}^p \\ \hline I_{\mathrm{VSD}}^q \end{bmatrix} \approx \left[\begin{array}{c|c} W_{\mathrm{VSD}}^{pp-M} & W_{\mathrm{VSD}}^{pq-M} \\ \hline W_{\mathrm{VSD}}^{qp-M} & W_{\mathrm{VSD}}^{qq-M} \end{array} \right] \begin{bmatrix} I^{p-\mathrm{dc}M} \\ \hline I^{q-\mathrm{dc}M} \end{bmatrix} \quad (18)$$

where the vector

$$I_{\mathrm{VSD}}^p = [\overbrace{I_5^p, I_7^p, I_{11}^p, \ldots}^{\text{M terms}}]^T$$

represents the ac-side, in-phase components uniquely consumed by the VSD, and the vector

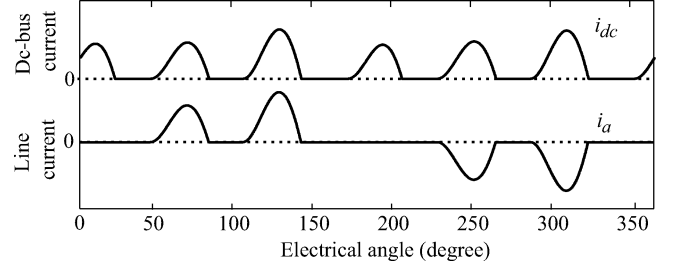$$I_{\mathrm{VSD}}^q = [\overbrace{I_5^q, I_7^q, I_{11}^q, \ldots}^{\text{M terms}}]^T$$

Fig. 7. Examples of dc-bus and ac-side current waveforms in a general case.

represents the ac-side, quadrature components uniquely consumed by the VSD. Matrices W_{VSD}^{pp-M}, W_{VSD}^{pq-M}, W_{VSD}^{qp-M}, and W_{VSD}^{qq-M} contain corresponding coefficients for the higher order current harmonics consumed by the VSD. Let

$$W_1^M = \left[\begin{array}{c|c} W_1^{pp-M} & W_1^{pq-M} \\ \hline W_1^{qp-M} & W_1^{qq-M} \end{array} \right] \quad (19)$$

and

$$W_{a-\mathrm{VSD}}^M = \left[\begin{array}{c|c} W_{\mathrm{VSD}}^{pp-M} & W_{\mathrm{VSD}}^{pq-M} \\ \hline W_{\mathrm{VSD}}^{qp-M} & W_{\mathrm{VSD}}^{qq-M} \end{array} \right] \quad (20)$$

and then the estimated fundamental harmonic components consumed by the VSD are given by

$$\begin{bmatrix} \widehat{I}_1^p \\ \hline \widehat{I}_1^q \end{bmatrix} = T_1 \begin{bmatrix} I_{\mathrm{VSD}}^p \\ \hline I_{\mathrm{VSD}}^q \end{bmatrix} \quad (21)$$

where $T_1 = W_1^M \left(W_{\mathrm{VSD}}^M \right)^{-1}$. Because the matrix W_{VSD}^M depends on the shifted angle α, it is possible that it could become nearly singular. However, the badly conditioned matrix can be tested off-line, and the problem can be mitigated by reducing the dimension of matrix W_{VSD}^M.

In general, the input voltage may be slightly unbalanced or distorted and the system may never reach steady state. As a result, each current pulse in the line cycle may be different as shown in Fig. 7. In this case, additional ac-side harmonics are required to accurately estimate the dc-side harmonics. Using the approximate switching function, triplen harmonics can be used to estimate additional even dc-side harmonics.

Let $I_x^{p-\mathrm{dc}} = [I_2^{p-\mathrm{dc}}, I_4^{p-\mathrm{dc}}, I_8^{p-\mathrm{dc}}, I_{10}^{p-\mathrm{dc}}]^T$ be additional dc-side harmonics to be considered. Other higher-order even harmonics are represented by $\Delta I_x^{p-\mathrm{dc}} = [I_{14}^{p-\mathrm{dc}}, I_{16}^{p-\mathrm{dc}}, I_{20}^{p-\mathrm{dc}}, \ldots]^T$. Additional ac-side harmonics used in the estimation are included in the vector $I_x^p = [I_3^p, I_9^p]^T$. Similar vectors can be written for the quadrature components, $I_x^{q-\mathrm{dc}} = [I_2^{q-\mathrm{dc}}, I_4^{q-\mathrm{dc}}, I_8^{q-\mathrm{dc}}, I_{10}^{q-\mathrm{dc}}]^T$, $\Delta I_x^{q-\mathrm{dc}} = [I_{14}^{q-\mathrm{dc}}, I_{16}^{q-\mathrm{dc}}, I_{20}^{q-\mathrm{dc}}, \ldots]^T$, and $I_x^q = [I_3^q, I_9^q]^T$. Additional dc-side harmonics change (17) and (18) to

$$\begin{bmatrix} I_1^p \\ \hline I_1^q \end{bmatrix} \approx W_1^M \begin{bmatrix} I^{p-\mathrm{dc}M} \\ \hline I^{q-\mathrm{dc}M} \end{bmatrix} + W_1^x \begin{bmatrix} I_x^{p-\mathrm{dc}} \\ \hline I_x^{q-\mathrm{dc}} \end{bmatrix} \quad (22)$$

and

$$\begin{bmatrix} I_{\text{VSD}}^p \\ I_{\text{VSD}}^q \end{bmatrix} \approx W_{\text{VSD}}^M \begin{bmatrix} I^{p-\text{dc}M} \\ I^{q-\text{dc}M} \end{bmatrix} + W_{\text{VSD}}^x \begin{bmatrix} I_x^{p-\text{dc}} \\ I_x^{q-\text{dc}} \end{bmatrix}. \quad (23)$$

A similar equation can be written for the triplen harmonics as

$$\begin{bmatrix} I_x^p \\ I_x^q \end{bmatrix} \approx W_x^x \begin{bmatrix} I_x^{p-\text{dc}} \\ I_x^{q-\text{dc}} \end{bmatrix}. \quad (24)$$

Matrices W_1^x, W_{VSD}^x, and W_x^x contain corresponding coefficients for the ac-side harmonics. The estimation error in the augmented system using the estimator derived in the balanced case is given by

$$\begin{bmatrix} e_1^p \\ e_1^q \end{bmatrix} = (\Delta W_1^M - T_1 \Delta W_{\text{VSD}}^M) \begin{bmatrix} \Delta I^{p-\text{dc}M} \\ \Delta I^{q-\text{dc}M} \end{bmatrix}$$
$$+ (W_1^x - T_1 W_{\text{VSD}}^x) \begin{bmatrix} I_x^{p-\text{dc}} \\ I_x^{q-\text{dc}} \end{bmatrix}$$
$$+ (\Delta W_1^x - T_1 \Delta W_{\text{VSD}}^x) \begin{bmatrix} \Delta I_x^{p-\text{dc}} \\ \Delta I_x^{q-\text{dc}} \end{bmatrix}. \quad (25)$$

Additional harmonics can be used to minimize the second error term, $(W_1^x - T_1 W_{\text{VSD}}^x)[I_x^{p-\text{dc}}, I_x^{q-\text{dc}}]^T$. The error correction factor is given as

$$T_1^x = \left(\left(W_x^x (W_x^x)^T \right)^{-1} \left(W_x^x (W_1^x - T_1 W_{\text{VSD}}^x)^T \right) \right)^T. \quad (26)$$

The final estimating function is

$$\begin{bmatrix} \widehat{I}_1^p \\ \widehat{I}_1^q \end{bmatrix} = T_1 \begin{bmatrix} I_{\text{VSD}}^p \\ I_{\text{VSD}}^q \end{bmatrix} + T_1^x \begin{bmatrix} I_x^p \\ I_x^q \end{bmatrix}. \quad (27)$$

Equation (27) provides a closed-form solution for estimating the fundamental current harmonic consumed by a three-phase rectifier from higher current harmonics. In addition, the algorithm does not require any prior knowledge of system parameters. The algorithm can be modified to use other sets of harmonics by changing the coefficient matrices.

VI. RESULTS AND DISCUSSION

This section summarizes experimental results that demonstrate the ability of the switching-function-based VSD power estimator to resolve the power consumption of VSD and rectifier loads from other constant power loads. In addition, the estimation results are compared with the empirically based estimator to compare the improvement.

The experimental setup consisted of a controllable three-phase voltage source and three electronic loads: a VSD system connected to a dynamometer, a 200-W three-phase rectifier load, and a 50-W light bulb connected between phase-A and neutral. The experimental setup is shown in Fig. 8.

For all experiments, the switching-function-based estimator used three in-phase and three quadrature components of ac-side harmonics, specifically, $I_{\text{VSD}}^p = [I_5^p, I_7^p, I_{11}^p]^T$ and $I_{\text{VSD}}^q = [I_5^q, I_7^q, I_{11}^q]^T$. In addition, the third and ninth harmonics were
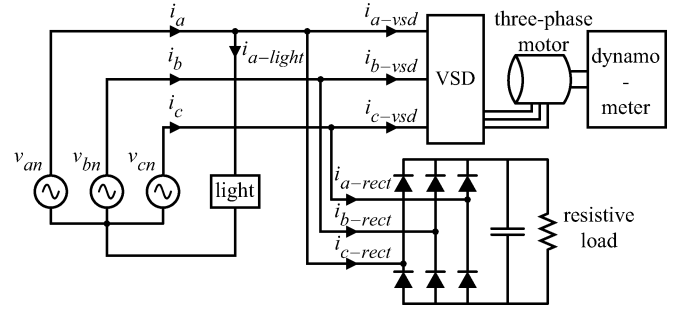

Fig. 8. Experimental setup.

used for the error correction factor, $I_x^p = [I_3^p, I_9^p]^T$ and $I_x^q = [I_3^q, I_9^q]^T$. The real power consumed by the VSD and the rectifier is calculated together using (5). The light bulb fundamental real power is calculated by

$$P_{1-\text{light}} = V_1^a (I_1^p - \widehat{I}_1^{pa}) \quad (28)$$

where V_1^a is the amplitude of the fundamental of phase-A line-to-neutral voltage and $\widehat{I}_1^{pa}$ represents the estimated fundamental current harmonic consumed by the VSD in phase-A.

A. Balanced Input Voltage Cases

First, the switching-function-based VSD power estimator was tested under a balanced input voltage case. This input voltage was used to generate the correlation function for the empirically based estimator. The goal of this test is to demonstrate the ability of the switching-function-based estimator to extract the power consumed by both the VSD and the rectifier from the 50-W light bulb during a sequence of load operations. Experimental results are shown in Fig. 9. Clearly that the switching-function-based estimator can resolve the power consumption of the VSD and the rectifier successfully when the input voltage is balanced. Small errors can be noticed during the light bulb start-up transient because the sharp transient contains higher current harmonics that are used as input variables to the VSD estimator. A more complex method may be applied to minimize the estimation error during transient events caused by other loads. On the other hand, the estimated light bulb power using the empirically based estimator is shown in Fig. 10. The result indicates that the empirically based estimator produces an error during the rectifier load operation.

B. Distorted Input Voltage Cases

To measure the performance of the proposed estimator under input voltage variation, different levels of input voltage distortion were imposed during the experiments to compare performance between the empirically-based and the switching-function-based estimators. In these tests, the VSD was running with constant load and the input voltage was distorted by different amounts of fifth or seventh harmonic in all three phases. The performance is measured by the percentage error of the
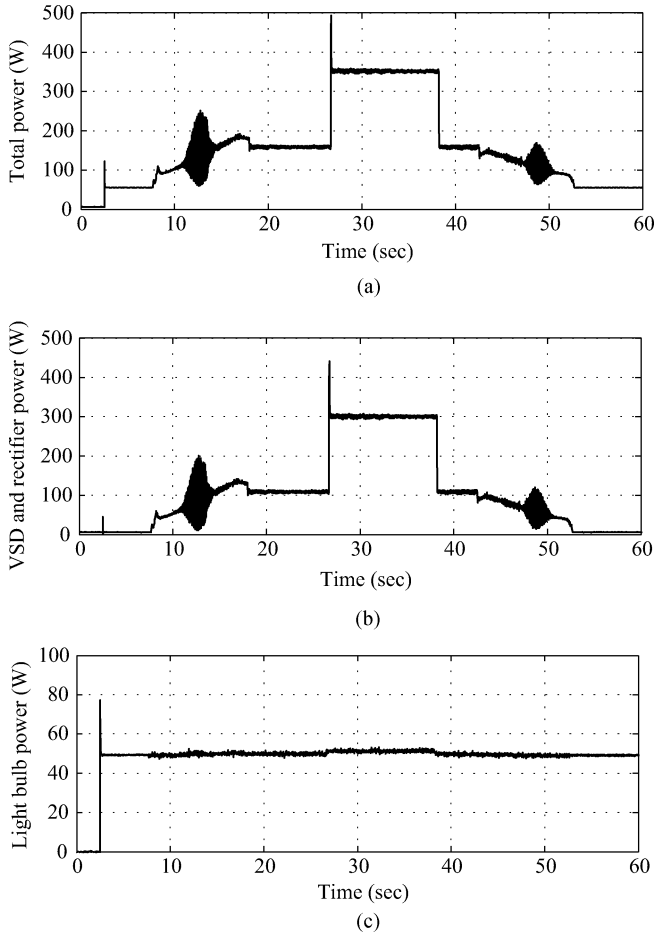
Fig. 9. Resolving power consumption of VSD and rectifier loads from the 50-W light bulb using the switching-function-based estimator under balanced input voltages; (a) Total power. (b) Power consumed by the VSD and the rectifier. (c) Power consumed by the 50-W light bulb.
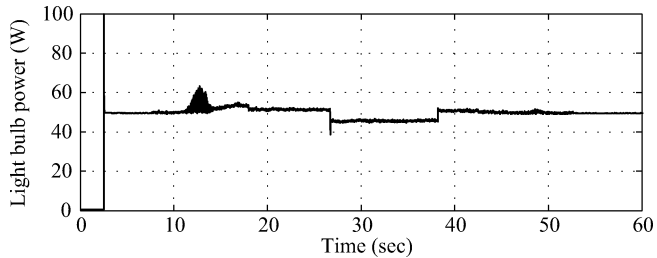

Fig. 10. Estimated power of the 50-W light bulb after the empirically based estimator has removed power of the VSD and the rectifier under balanced input voltages.

estimated VSD real power consumption, specifically

$$\%\text{error} = \frac{|P_{1\text{-VSD}} - \widehat{P}_{1\text{-VSD}}|}{P_{1\text{-VSD}}} \times 100.$$

The experimental results are shown in Figs. 11 and 12.

The experimental results demonstrate that the switching-function-based algorithm is robust against input voltage distortion across a wide load range. This improvement confirms that the approximation made during the derivation is valid for small voltage distortions that are likely to occur in the field.
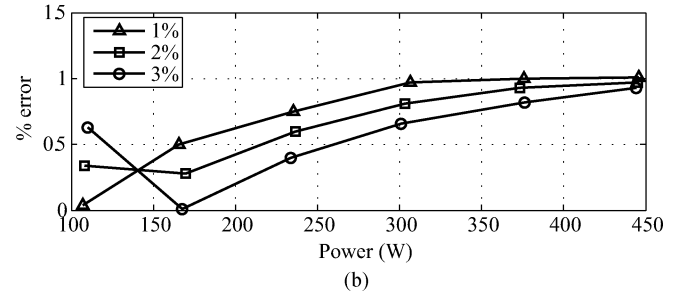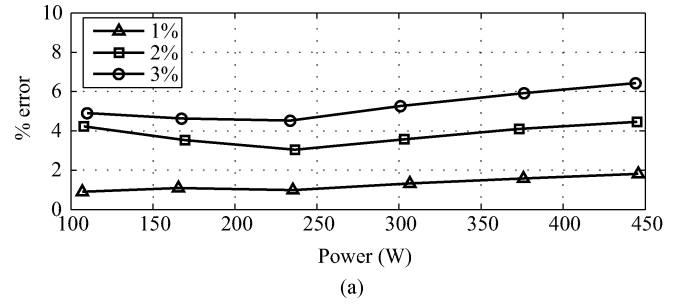

Fig. 11. Estimation error percentages of VSD power estimators when the input voltages are distorted with different levels of fifth harmonic. (a) Empirically based estimator. (b) Switching-function-based estimator.
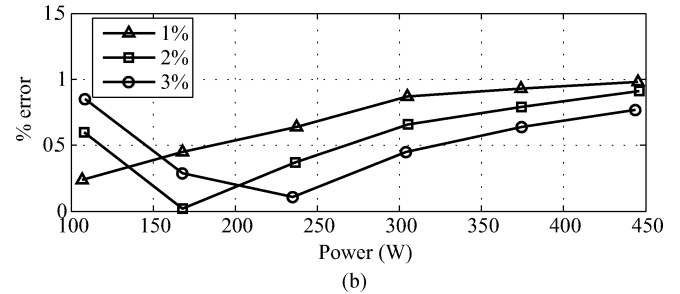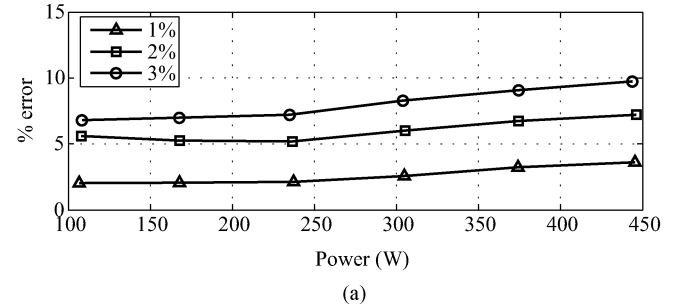

Fig. 12. Estimation error percentages of VSD power estimators when the input voltages are distorted with different levels of seventh harmonic. (a) Empirically based estimator. (b) Switching-function-based estimator.

VII. CONCLUSION

This paper has demonstrated the method to extract the fundamental current harmonic of the uncontrolled, three-phase rectifier load using a linear combination of higher ac-side harmonics. The proposed estimator does not require the complete knowledge of circuit parameters and the system's operating point. The experimental results demonstrate that the switching-function-based VSD power estimator shows significant improvement over the empirically based estimator in resolving the VSD power

consumption under small variations in the input voltage. The proposed algorithm enables NILM to work with a larger set of loads. Furthermore, the estimator also shows the ability to track multiple VSDs and rectifier loads together without an additional sensor. This method could be adapted to track other nonlinear loads as well.

We are working to extend the approach taken in this paper to other monitoring and modeling problems. For example, even in drives that incorporate harmonic filters, it may be possible to develop functions that relate filtered but still detectable harmonic components to real power consumption. In drives that incorporate active power factor correction, it appears possible to relate harmonic content due to crossover distortion or switch frequency modulation of harmonic components to the real power consumed by a drive. Where possible, the approach of identifying mathematical models and functional dependencies between any observable harmonic and other quantities of interest like real or reactive power enables "smart" monitoring applications like the one described in this paper.

APPENDIX

COMPUTATIONS OF SWITCHING-FUNCTION WEIGHTING COEFFICIENTS

The dc-component of the line current is given in (11) as

$$I_0 = W_0^{0p} I^{p-\mathrm{dc}} + W_0^{0q} I^{q-\mathrm{dc}}$$

where W_0^{0p} and W_0^{0q} are the row vectors of the switching-function coefficients. Matrices W_0^{0p} and W_0^{0q} can be written as

$$W_0^{0p} = \begin{bmatrix} S_0 & -\frac{1}{2}S_1^q & -\frac{1}{2}S_2^q & -\frac{1}{2}S_3^q & \dots \end{bmatrix} \tag{29}$$

and

$$W_0^{0q} = \begin{bmatrix} \frac{1}{2}S_1^p & \frac{1}{2}S_2^p & \frac{1}{2}S_3^p & \dots \end{bmatrix}. \tag{30}$$

The in-phase component of the kth line current harmonic is given in (12) as

$$I_k^p = W_k^{pp} I^{p-\mathrm{dc}} + W_k^{pq} I^{q-\mathrm{dc}}$$

where the quantities W_k^{pp} and W_k^{pq} are row vectors. The vector W_k^{pp} can be represented as

$$W_k^{pp} = \begin{bmatrix} w_{k,0}^{pp} & w_{k,1}^{pp} & w_{k,2}^{pp} & \dots \end{bmatrix}. \tag{31}$$

Each coefficient of the matrix $w_{ap}^A(k,m)$ can be computed as

$$w_{k,m}^{pp} = \begin{cases} S_k^p, & \text{for } m = 0 & \text{(32a)} \\ \frac{1}{2}(S_{m+k}^p + S_{k-m}^p), & \text{for } m < k & \text{(32b)} \\ \frac{1}{2}S_{m+k}^p + S_0, & \text{for } m = k & \text{(32c)} \\ \frac{1}{2}(S_{m+k}^p - S_{m-k}^p), & \text{for } m > k & \text{(32d)} \end{cases}$$

where the variable m represents the dc-side harmonic number, i.e., $m = 0, 1, 2, \dots$. The dc component is denoted by $m = 0$.

Similarly, the vector W_k^{pq} can be represented as

$$W_k^{pq} = \begin{bmatrix} w_{k,1}^{pq} & w_{k,2}^{pq} & w_{k,3}^{pq} & \dots \end{bmatrix}. \tag{33}$$

Each coefficient of the matrix $w_{k,m}^{pq}$ can be computed as

$$w_{k,m}^{pq} = \begin{cases} \frac{1}{2}(S_{m+k}^q - S_{|m-k|}^q), & \text{for } m \neq k & \text{(34a)} \\ \frac{1}{2}S_{m+k}^q + S_0, & \text{for } m = k. & \text{(34b)} \end{cases}$$

The quadrature component is given in (13) as

$$I_k^q = W_k^{qp} I^{p-\mathrm{dc}} + W_k^{qq} I^{q-\mathrm{d}}$$

where the quantities W_k^{qp} and W_k^{qq} are row vectors. The vector W_k^{qp} can be represented as

$$W_k^{qp} = \begin{bmatrix} w_{k,0}^{qp} & w_{k,1}^{pq} & w_{k,2}^{pq} & \dots \end{bmatrix}. \tag{35}$$

Each coefficient of the matrix $w_{k,m}^{qp}$ can be computed as

$$w_{k,m}^{qp} = \begin{cases} S_k^q, & \text{for } m = 0 & \text{(36a)} \\ \frac{1}{2}(S_{m+k}^q + S_{|m-k|}^q), & \text{for } m \neq k & \text{(36b)} \\ \frac{1}{2}S_{m+k}^q - S_0, & \text{for } m = k. & \text{(36c)} \end{cases}$$

Similarly, the vector W_k^{qq} can be represented as

$$W_k^{qq} = \begin{bmatrix} w_{k,1}^{qq} & w_{k,2}^{qq} & w_{k,3}^{qq} & \dots \end{bmatrix}. \tag{37}$$

Each coefficient of the matrix $w_{k,m}^{qq}$ can be computed as

$$w_{k,m}^{qq} = \begin{cases} -\frac{1}{2}(S_{m+k}^p - S_{k-m}^p), & \text{for } m < k & \text{(38a)} \\ -\frac{1}{2}S_{m+k}^p - S_0, & \text{for } m = k & \text{(38b)} \\ -\frac{1}{2}(S_{m+k}^p + S_{m-k}^p), & \text{for } m > k. & \text{(38c)} \end{cases}$$
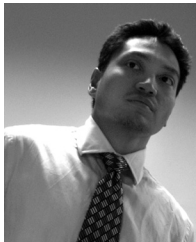
REFERENCES

[1] S. W. D. Haan, "Analysis of the effect of source voltage fluctuations on the power factor in three-phase controlled rectifiers," *IEEE Trans. Ind. Appl.*, vol. IA-22, no. 2, pp. 259–266, Mar. 1986.
[2] Y. Baghzouz, "An accurate solution to line harmonic distortion produced by ac/dc converters with overlap and dc ripple," *IEEE Trans. Ind. Appl.*, vol. 29, no. 3, pp. 536–540, May/Jun. 1993.
[3] M. Sakui and H. Fujita, "An analytical method for calculating harmonic currents of a three-phase diode bridge rectifier with dc filter," *IEEE Trans. Power Electron.*, vol. 9, no. 6, pp. 631–637, Nov. 1994.
[4] D. E. Rice, "A detailed analysis of six-pulse converter harmonic currents," *IEEE Trans. Ind. Appl.*, vol. 30, no. 2, pp. 294–304, Mar./Apr. 1994.
[5] W. Xu, H. W. Dommel, M. B. Hughes, G. W. Chang, and L. Tan, "Modelling of adjustable speed drives for power system harmonic analysis," *IEEE Trans. Power Del.*, vol. 14, no. 2, pp. 595–601, Apr. 1999.
[6] M. Grötzbach and R. Redmann, "Line current harmonics of VSI-fed adjustable-speed drive," *IEEE Trans. Ind. Appl.*, vol. 36, no. 2, pp. 683–690, Mar./Apr. 2000.
[7] M. Grötzbach and M. Bauta, "Modeling of ac/dc converters under unbalanced voltage supply using complex switching functions," in *Proc. Harmon. Quality Power*, Nov. 2002, vol. 2, pp. 710–715.
[8] V. Caliskan, D. J. Perreault, T. M. Jahns, and J. G. Kassakian, "Analysis of three-phase rectifiers with constant-voltage loads," *IEEE Trans. Circuits Syst.*, vol. 50, no. 9, pp. 1220–1226, Nov. 2003.
[9] F. Wang, G. Chen, D. Boroyevish, S. Ragon, M. Arpilliere, and V. R. Stefanovic, "Analysis and design optimization of diode front-end rectifier passive components for voltage source inverters," *IEEE Trans. Power Electron.*, vol. 23, no. 5, pp. 2278–2289, Sep. 2008.

[10] K. D. Lee, "Electric load information system based on non-intrusive power monitoring," Ph.D. dissertation, Mass. Inst. of Tech., Cambridge, MA, Jun. 2003.

[11] K. D. Lee, S. B. Leeb, L. K. Norford, P. R. Armstrong, J. Holloway, and S. R. Shaw, "Estimation of variable-speed-drive power consumption from harmonic content," *IEEE Trans. Energy Convers.*, vol. 20, no. 3, pp. 566–574, Sep. 2005.

[12] S. B. Leeb, S. R. Shaw, and J. L. Kirtley, "Transient event detection in spectral envelope estimates for nonintrusive load monitoring," *IEEE Trans. Power Del.*, vol. 10, no. 3, pp. 1200–1210, Jul. 1995.

[13] A. Cole and A. Albicki, "Nonintrusive identification of electrical loads in a three-phase environment based on harmonic content," in *Proc. IMTC 2000*, May, vol. 1, pp. 24–29.

[14] S. R. Shaw and C. Laughman, "A kalman-filter spectral envelope preprocessor," *IEEE Trans. Instrum. Meas.*, vol. 56, no. 5, pp. 2010–2017, Oct. 2007.

Robert W. Cox (S'01–M'06) received the Ph.D. degree in electrical engineering and computer science from Massachusetts Institute of Technology, Cambridge, in 2006.

He is currently an Assistant Professor with the Department of Electrical and Computer Engineering, University of North Carolina, Charlotte. His current research interests include sensing and measurement problems for various diagnostic applications in power systems.

Warit Wichakool (S'05) received the S.B. and M.Eng. degrees in electrical engineering and computer science from Massachusetts Institute of Technology (MIT), Cambridge, in 2001. He is currently working toward the Ph.D. degree in electrical engineering at the Laboratory for Electromagnetic and Electronic Systems, MIT.

His current research interests include system modeling, circuit design, and signal processing for power electronics applications.

Steven B. Leeb (F'07) received the doctoral degree in electrical engineering and computer science from Massachusetts Institute of Technology (MIT), Cambridge, in 1993.

He has been with the Department of Electrical Engineering and Computer Science, MIT, since 1993. He is currently a Professor at the Laboratory for Electromagnetic and Electronic Systems, MIT, where he is engaged in the design, analysis, development, and maintenance processes for all kinds of machinery with electrical actuators, sensors, or power electronic drives.

Al-Thaddeus Avestruz (S'04) received the S.B. degree in physics and the S.M. and E.E. degrees, in 1994, and 2006, respectively from Massachusetts Institute of Technology (MIT), Cambridge. He is currently working toward the Ph.D. degree in electrical engineering at the Laboratory for Electromagnetic and Electronic Systems, MIT.

He was with several companies, including Teradyne Corporation, North Reading, MA, Thornton, Inc. (presently Mettler-Toledo Thornton, Capitol Heights, MD), and Diversified Technologies, Inc., Augusta, GA, before returning to MIT. His current research interests include circuit design, power conversion, energy, and electromagnetic systems.